Proceedings of the 10th World Congress on New Technologies (NewTech'24)
Barcelona, Spain - August 25-27, 2024
Paper No. ICCEIA 134
DOI: 10.11159/icceia24.134

Analysing the Impact of Basalt Fiber Concrete on Continuous Beams Reinforced with BFRP Bars through Numerical Simulation

Samar Alsaleh[1], Osama Mohamed [1]
[1] College of Engineering, Abu Dhabi University
Abu Dhabi, UAE
1082449@students.adu.ac.ae; Osama.Mohamed@adu.ac.ae

Abstract
The difference in flexural response of concrete beams due to reinforcement with conventional steel versus basalt fibre reinforced polymer (BFRP) bars was studied using finite element models that were validated using experimental data. In addition, the effect of basalt fibres on flexural response of beams reinforced with conventional steel or with BFRP bars was evaluated in each of the two cases. The commercial software ABAQUS was conducted to develop the finite element models and conduct the analysis. The effect of shear reinforcement on structural response was incorporated using two steel stirrup spacings. A total of 11 models were created to capture the effect of steel reinforcement ratio, BFRP reinforcement ratio, basalt fibres volume fraction, and stirrup spacings. Incorporating basalt fibres improves the beams ductility index and load-carrying capacity in both steel-reinforced and BFRP-reinforced beams. The reinforcement ratio for top and bottom reinforcement and stirrups spacing have a noticeable effect on failure mode and cracks distribution. Numerical models were able to success in simulating experimental tests for all beams.

***Keywords*:** basalt FRP bars, basalt fibres, concrete damaged plasticity, bond strength, finite element, reinforced concrete.

1. Introduction

Basalt fibers are gaining popularity in industry due to their functional properties such as the unique thermal and fire insulation and high temperature resistance [1,2]. Basalt fibres are generally biocompatible with no chemical component added and a simple manufacture approach. Basalt fibres are recyclable, therefore, are eco-friendly and sustainable alternative [3]. Due to their light weight and high strength, basalt fibres are used in the production of structural elements in aerospace, and automotive industries [4,5].

Unlike conventional concrete reinforcing steel, basalt fibre reinforced polymer (BFRP) bars exhibit linear elastic behaviour in tension up to failure. Therefore, when BFRP bars are used as reinforcing steel, concrete flexural elements can suddenly fail without sufficient warning [6]. Failure in concrete beams reinforced with BFRP bars appears as sever concrete spalling and critical diagonal cracks in a flexure-shear combined failure when stresses reach the peak compressive strength [7]. Comprehensive discussion of flexural strength, overall capacity, and durability of concrete beams and slabs reinforced with BFRP bars is provided in the literature [8, 9].

Continuous reinforced concrete beams are commonly used structural system due to their ability to redistribute moment and forces from lower to higher stiffness sections, which improves their ductility and rotational capacity. However, BFRP reinforcing bars may affect the behaviour and reduce the ductility of structural elements [10]. Therefore, use of high strength concrete with FRP reinforcement was attempted to allow the stiffness of the cracked concrete to be compatible with the high stress and strain properties of FRP bars [11,12]. When added to concrete during mixing, basalt fibres provide confinement and bridging effects to the concrete that may limit crack width and control deformations, therefore, increases concrete capacity [13,7]. The volume fraction and type of basalt fibres added to the concrete mix influences tensile strength and to some extent compressive strength of concrete [14]. It is therefore essential to develop a compressive understanding of the fibre composites interaction with structural elements and develop credible analytical models to predict its behavior.

2. Details of models' specimens

Finite element simulations and models were created using the commercial program ABAQUS. Experimental validation of numerical results was based tests reported by Abushanab et al. [15]. Three groups of concrete beams have been

compared. The same geometric properties and material characteristics were adopted for groups B1, B2 & B3. The response of groups in terms of mechanical properties and failure modes for various reinforcement ratios, arrangement, shear reinforcement spacing, and basalt volume fraction was compared.

Group B1 represents ordinary, medium strength concrete and includes two standard beams reinforced with steel rebars, and three beams reinforced with BFRP with various top and bottom reinforcement and two spacings of transverse reinforcement, as shown in Table 1. The models in groups B2 & B3 represent beams from group B1 but include two different volume fractions of basalt fibres, V_f.

Table 1: Properties of simulation models

Group	Beam	Reinforcement Type	V_f of BMF	Bottom reinforcement	Top reinforcement	Transverse reinforcement spacing (mm)
1	B1-S-1	steel rebar	0%	4 ø 12	3 ø 12	120
	B1-S-2	steel rebar	0%	4 ø 12	3 ø 12	80
	B1-B-1	BFRP bars	0%	6 ø 10	4 ø 10	120
	B1-B-2	BFRP bars	0%	6 ø 10	6 ø 10	120
	B1-B-3	BFRP bars	0%	6 ø 10	4 ø 10	80
2	B2-S-1	steel rebar	0.75%	4 ø 12	3 ø 12	120
	B2-B-1	BFRP bars	0.75%	6 ø 10	4 ø 10	120
	B2-B-2	BFRP bars	0.75%	6 ø 10	6 ø 10	120
	B2-B-3	BFRP bars	0.75%	6 ø 10	4 ø 10	80
3	B3-S-1	steel rebar	1.50%	4 ø 12	3 ø 12	120
	B3-B-1	BFRP bars	1.50%	6 ø 10	4 ø 10	120

The tested beams were each 4-meters in total length divided into two continuous spans, with a constant cross-section of 200 × 300 mm, as shown in figure 1. A constant concrete cover of 25mm was provided for the reinforcement in all beams. The beams were longitudinally reinforced with steel or BFRP bars. In addition, 10-mm diameter steel bars with yield tensile strength of 515 MPa, and yield strain of 0.00267 were used as transverse reinforcement for all beams.

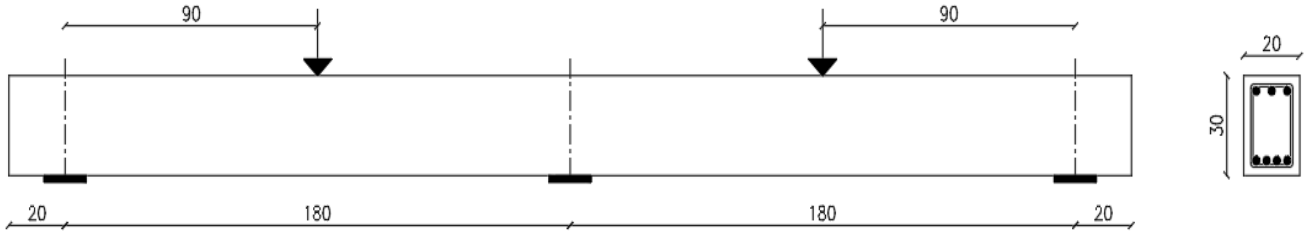

Fig. 1: Longitudinal view and section in beam

3. Material properties

3.1. Concrete Damage Plasticity Model

In the finite element models implemented in this study, a concrete damage plasticity (CDP) was used to simulate the compression and tension damage in concrete using plasticity and damage mechanics theories [16]. Concrete damage is represented by crushing in compression areas and cracking in tension area, caused by the material hardening and softening behaviour that is accompanied by degradation in elastic stiffness and growth of yield surface [17].

The elastic part of the concrete stress strain curve is defined by modulus of elasticity (*E)*, and Poisson's ratio (υ). Tensile strength (f_{tu}), initial strain (ε_o), and its associate compressive strength (f_{cu}) presented in table 2 are used to generate the plastic and damage behaviour. ACI-318 uses equation 1 to represent the elastic modulus of normal weight concrete as a function of concrete compressive strength ($\acute{f}_c$). To approximate plastic behaviour, concrete is simulated as an isotropic material using plasticity parameters. Compression and tension damage is reflected by the inelastic stress-strain data under compression and cracking stress-strain data under tension [17]. The plasticity flow parameters, shown in table 3, could be specified by either experimental tests or existing constitutive models. In table 3, ψ refers to the Dilation angle, $\in$ is the Eccentricity, K is the ratio of second stress invariant to tensile meridian, f_{bo}/f_{co} is the compressive plasticity deformation, and μ is viscosity Parameter [18, 19].

$$E = 4700\sqrt{f_c'} \qquad (1)$$

Table 2: Mechanical properties for normal concrete, without basalt fibres ($V_f = 0$)

E (MPa)	υ	f_{cu} (MPa)	f_{tu} (MPa)	ε_o
29497.88297	0.182	39.39	4.1	0.0019

Table 3: Concrete damaged plasticity parameters (CDP)

ψ	$\in$	f_{bo}/f_{co}	K	μ
35	0.1	1.16	0.67	0.0001

When fibres, including basalt fibres are mixed with concrete, they alter several fresh and hardened properties of concrete structural elements [14]. The effect of fibres on fresh and mechanical properties of concrete depends on several fibre-related factors such as the fibre length/diameter ratio, fibre type, and the content of fibres usually as described a volume fraction, V_f, or as ratio of fibre to binder weight. Three types of concrete materials were used in this study with different volume fractions, V_f, of basalt fibers. The fibre volume fraction used are $V_f = 0$, 0.75%, and 1.5%. It was reported that added fibres within practical limits have limited effect on concrete compressive strength, however it has a remarkable effect on tensile strength, strain capacity, and toughness [14, 20].

Equation 2 is used to generate the elastic part of the stress-strain curve till stresses reaches the ultimate compressive stress, where $0 \leq \varepsilon_c \leq \varepsilon_{c,lim}$ [21]. Then stress starts to decrease till concrete eventually fails at the ultimate strain, ε_{cu} [22]. Equation 3 is used for concrete without added fibres, while equation 4 represents concrete with basalt fibre, where $\varepsilon_{cf} \geq \varepsilon_{cf,lim}$ [21].

$$\sigma_{cf} = \frac{n\beta\sigma_c' \left(\frac{\varepsilon_c}{\varepsilon_o}\right)}{n\beta - 1 + \left(\frac{\varepsilon_c}{\varepsilon_o}\right)^{n\beta}} \qquad (2)$$

$$\sigma_c = \frac{\sigma_{c.lim}}{1 + 0.1(n-1)\left[\frac{\left\{\frac{\varepsilon_c}{\varepsilon'_c} - 1\right\}}{\left\{\frac{\varepsilon_{c,lim}}{\varepsilon'_c} - 1\right\}}\right]^{\{1+0.1(n-1)\}}} \qquad (3)$$

$$\sigma_c = \sigma_{cf,lim} \times \exp\left[\left(1 - n + 0.1{V_f}^2\right) \times \left\{\frac{\varepsilon_{cf}}{\varepsilon'_{cf}} - \frac{\varepsilon_{cf,lim}}{\varepsilon'_{cf}}\right\}^{1-0.1V_f}\right] \qquad (4)$$

Where:

β is a material parameter depending on the shape of the stress-strain curve.

For concrete without fibers $\beta = \left(\frac{\sigma'_c}{65.23}\right)^3 + 2.59$

For concrete with basalt fibre $\beta = \frac{1}{1-\left(\frac{E_{cf}}{E_{it}}\right)}$ [21]

$n = 0.21 + 0.07f'_c$ the toughness of the curve, measured by the area under the stress-strain curve to fracture [23]

σ'_c and ε'_c are the maximum compressive strengths and its corresponding strain.

$\varepsilon_{c,lim}$ limiting strain corresponding to the limiting stress ($\sigma_{c,lim}$) in the post-peak branch of the stress-strain curve

E_{cf} is the secant modulus of elasticity $\sigma'_{cf}/\varepsilon_{of}$

$E_{it} = \left(10300 - 400V_f\right)\sqrt[3]{\sigma'_{cf}}$ (in MPa) the initial tangent modulus [21]

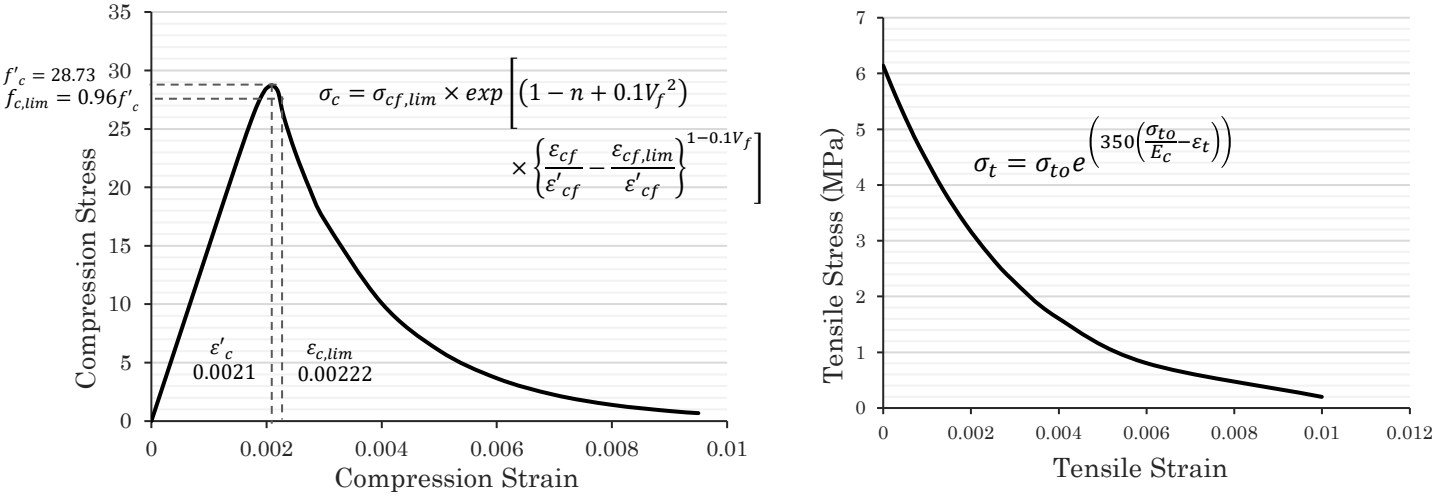

Fig. 2: Stress-strain curve for BFR concrete ($V_f = 0.75$)

The stress-strain ($\sigma_t - \varepsilon_t$) behaviour in tension is modelled using equation 5 [24].

$$\sigma_t = \sigma_{to}e^{\left(350\left(\frac{\sigma_{to}}{E_c} - \varepsilon_t\right)\right)} \qquad (5)$$

Where σ_{to} is the initial tensile stress.

The concrete plastic strain, ε_c^{pl}, is computed using equation 6 in ABAQUS software.

$$\varepsilon_c^{pl} = \varepsilon_c^{in} - \frac{d_c}{(1 - d_c)E_o}\frac{\sigma_c}{E_o} \qquad (6)$$

Where:

The damage parameter $d_c = 1 - \frac{\sigma_i}{\sigma_{cu}}$

The inelastic strain $\varepsilon_c^{in} = \varepsilon_c - \varepsilon_{oc}^{el}$

The elastic strain $\varepsilon_{oc}^{el} = \frac{\sigma_c}{E_o}$

3.2. Fibre Reinforced Polymer (FRP) bars

FRP bars are known to exhibit an elastic behaviour with sudden and brittle rupture when its tensile strength is exceeded [25]. FRP is an orthotropic material with different mechanical properties along the perpendicular axes [26]. When fibre reinforced composites are loaded in tension, stresses transfer elasticity from the matrix and distribute within the fibre along its axial direction [27]. The alignment of fibres in FRP bars ensure that the tensile strength is highest along the longitudinal

axis compared to the transverse directions. FRP bars are modelled as linear elastic isotropic material with a brittle failure when the ultimate tensile strength is reached [28,29]. Therefore, Hooke's law may be used based on the mechanical properties given in table 4 to represent the stress-strain behaviour of BFRP bars as shown in figure 5.

Table 4: Material properties of BFRP rebars

	Density (N/mm3)	E_f (GPa)	ε_{fu}	f_{fu} (MPa)
BFRP Y10	1.96E-05	44.7	0.023	1070

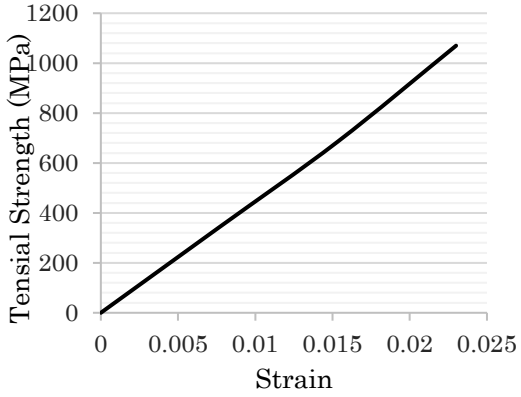

Fig. 5: BFRP stress-strain behaviour

3.3. Steel Reinforcing Bars

Steel is generally defined as an elastic-perfectly plastic material with properties that are similar in tension and compression. The parameters used to define the elastic and plastic responses in ABAQUS that are shown in table 5 are nominal stress-strain data generated from equations 7 and 8. Table 5 also shows types of steel used in the study, modulus of elasticity (E_s), yield strength (f_y) and ultimate tensile strength (f_u) [24].

$$\sigma_{true} = \sigma_{nom}(1 + \varepsilon_{nom}) \quad (7)$$

$$\varepsilon_{In}^{pl} = In(1 + \varepsilon_{nom}) - \sigma_{true}/E_s \quad (8)$$

Where:
σ_{true} is the true stress,
ε_{In}^{pl} is the plastic strain.
σ_{nom} and ε_{nom} are the nominal stress and nominal strain [30].

Table 5: Material properties of steel rebars

	Density (N/mm3)	E_s (MPa)	ε_y	ε_u	f_y (MPa)	f_u (MPa)
Steel (Y10)	7.85E-05	195000	0.00267	0.249	515	553
Steel (Y12)	7.85E-05	195000	0.00268	0.248	520	556

4. Finite element simulations

The methodology and selection of elements for finite elements are critical to obtain reliable predictions. Therefore, simulations were conducted consistent with ABAQUS manual and relevant literature. The beams were subjected to a uniform static pressure of 1unit/step at the locations shown in figure 1, until failure occurred. A concrete damage plasticity model (CDP) was used to define the compressive and tensile damage behaviour as discussed earlier in this article. The finite element

model used the standard ABAQUS C3D8R to represent the concrete, which is a three-dimensional 8-node linear brick element with second order reduced integration to avoid hourglassing and shear locking [31]. Tow-node linear beam elements were used to simulate the reinforcing steel and BFRP bars. A static general step was used in the analysis with a time-period equals to 1. To match the actual experiment boundary conditions, pinned supports were defined at the support point of the beam [4,22].

To enhance accuracy, a finer mesh enhances simulation effectiveness but increases the analysis time [32]. Therefore, a mesh size of 25 mm was adopted in this model and lead to reasonable results. A realistic bond model is necessary to represent the interaction and load-transfer between reinforcing bars and surrounding concrete. In this context, a confined bond model is typically necessary to simulate a realistic response of reinforced concrete flexural members [24]. Direct pull-out tests showed that when adequate pull-out strength is obtained on a deformed reinforcement bar, shear cracks appear at the surrounding concrete, followed by a pull-through failure. The confining concrete provides shear strength between the interlaminar that allows the reinforcement bar to achieve maximum bond strength [33]. In this study, a perfect bond will be considered where slippage between steel and concrete is prevented. The two materials are modelled so they have the same defined nodes by using link element to connect the nodes [22,34], which is achieved in ABAQUS by defining an *embedded region* constraint. Reinforcement bars are considered as the embedded member and concrete as a host region.

The ABAQUS 'Surface-to-surface' command was used to simulate the contact between concrete bottom and the supporting plate, and between concrete top surface and loading lines. The ABAQUS *hard contact* was used as the *interaction property* in normal direction and a common friction coefficient of 0.3 was used in the tangential direction.

5. Results and discussion

Analysis was conducted by subjecting the beams to static loads until the complete failure occurred, as described earlier. It was noted in all beams reinforced with steel bars that flexural failure occurs when the stress of the reinforcing rebar reaches the maximum tension capacity and concrete bending stress exceeds the section capacity. On the other hand, when BFRP-reinforced beams fail in flexure, it occurs suddenly when the compression strain exceeds critical strain. Crack appears as a warning before failure due to tension stresses in reinforced beams. In steel reinforced beams cracks spread and expand on a wider surface area than in BFRP beams as shown in figure6, which agrees with published literature[15]. The damage contours in figure 6 illustrate the crushing at compression zone and cracking at tension areas over beam length to different specimens.

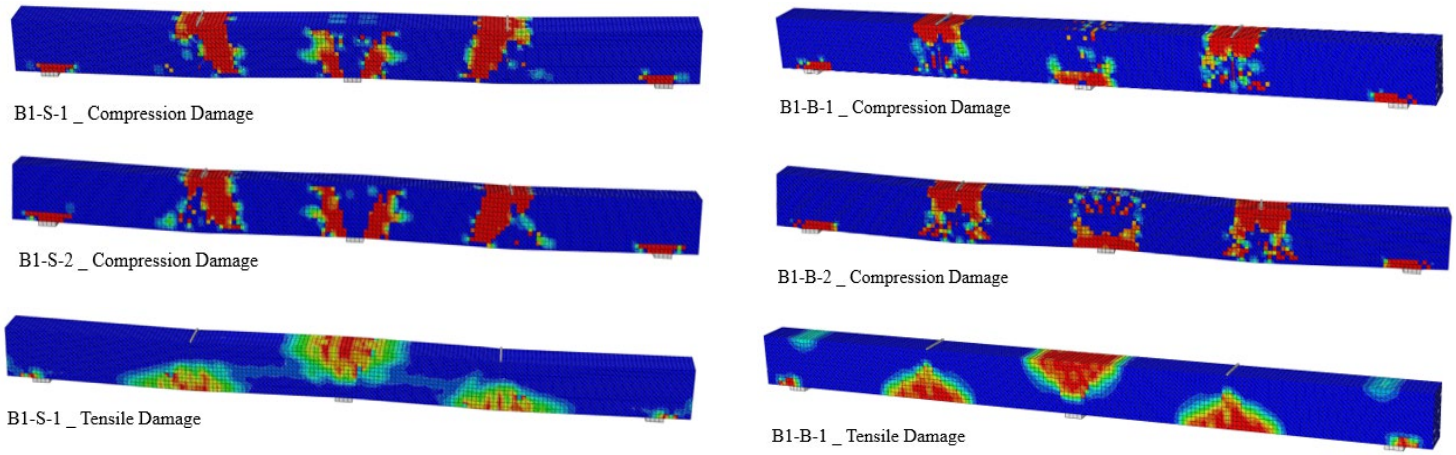

Fig. 6: Failure modes in simulation beam

It can be realized that in beam B1-B-1 the BFRP were able to transfer the failure from rupture of bars in the control beam to concrete crushing by showing a brittle elastic behaviour with no softening before failure, which is also noted in figures 7 & 8.

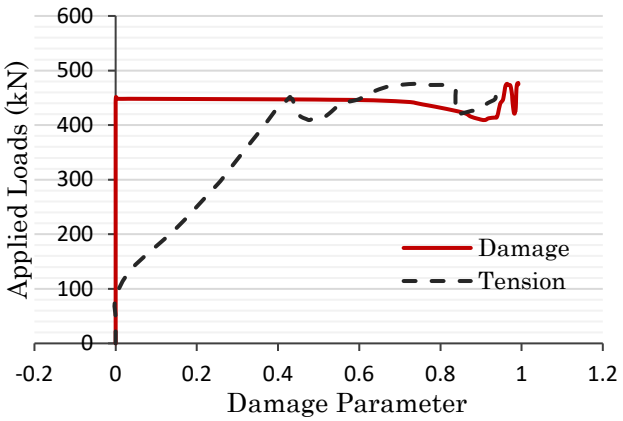

Fig. 7: Damage - Loads curve (B1-S-1)

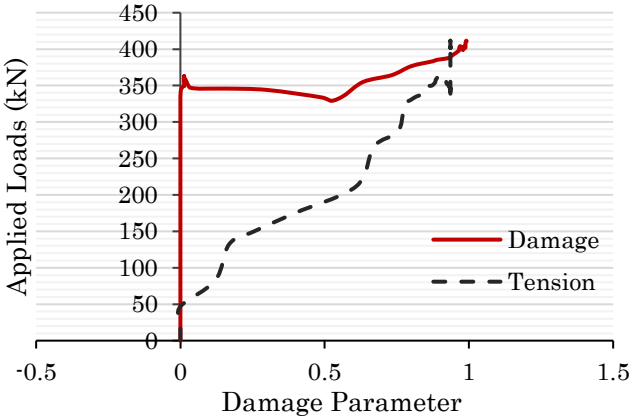

Fig. 8: Damage - Loads curve for (B1-B-1)

Beam B2-S-1 (BFRC), which included basalt files, experienced a flexure and flexure-shear failure, which helps in transferring the failure from splitting tensile failure to shear type failure. Therefore, using both basalt fibres in concrete and basalt reinforcement bars in B2-B-1 & B2-B-2 transfers the failure completely to shear failure as shown in figure 9.
The load-deflection relationship mainly depends on the type of reinforcement and the axial stiffness of the rebars. The smallest displacement value at failure was recorded for the steel reinforced beams. Models reinforced with BFRP bars showed wider range and higher displacement value than steel-reinforced beams, but it also showed lower load capacity, which is consistent with findings in literature [35,36]. The displacement range for the normal concrete specimen reinforced with steel rebars is 20-23mm with approximately corresponding forces of 480kN. The specimen reinforced with BFRP rebars range from 30-35mm with approximately 400kN load capacity. However, beams reinforced with basalt fibres show the best performance under the applied static load, the maximum range of displacements, and largest load capacity. The relation between the applied load and deflection of beams supplemented with basalt fibres and with BFRP or steel bars is shown in figure 11. A miner improvement in structural behaviour was observed in beams with smaller stirrup spacing and top to bottom reinforcement ratio equals to 1 as documented in the literature [15] and shown in figure 10.

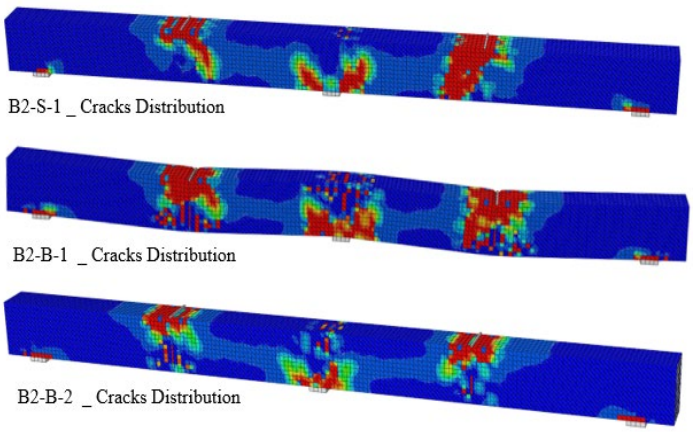

Fig. 9: Cracks distribution & Failure modes in beams

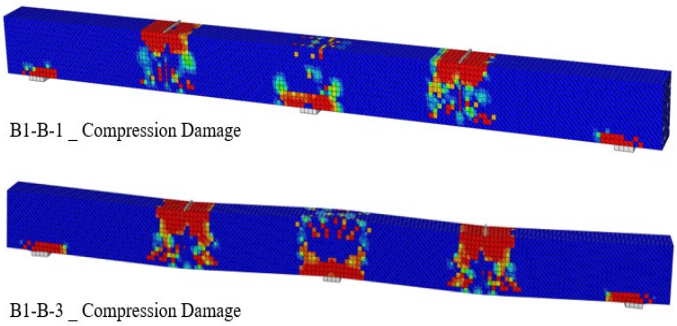

Fig. 10: Failure modes in beams

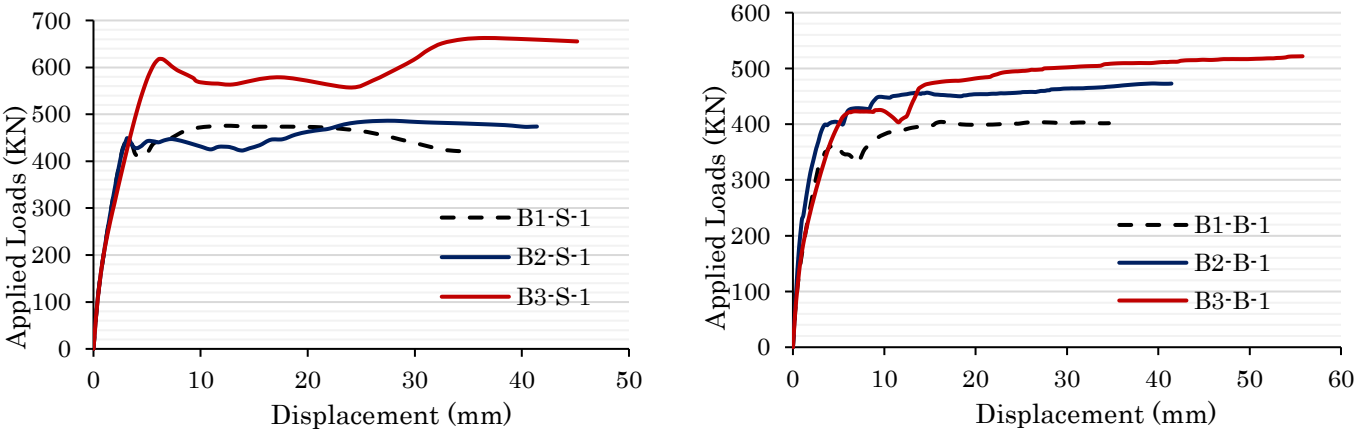

Fig. 11: The relation between applied loads and mid-span displacement

6. Conclusion

The study evaluated flexural response of concrete beams reinforced with either conventional elastoplastic steel bars or basalt fibre reinforced polymer (BFRP) bars and the influence on flexure and deformation is compared. In addition, adding basalt fibres to the concrete on structural response is compared in the cases when beams are reinforced with steel or BFRP bars. The comparison of results was based on failure mechanism, load-carrying capacity, and load-deflection response. The essential parameters included reinforced type (steel or BFRP), reinforcement ratio, basalt fibre ratio. Numerical modelling was conducted using the finite element method and results were validated using test results published in the literature.

The use of basalt fibres increases both the axial load-carrying capacity and ductility of beams reinforced with steel or with BFRP bars.

References

[1] O.H. Zinkaah, Z. Alridha & M. Alhawat, "Numerical and theoretical analysis of FRP reinforced geopolymer concrete beams," in *Construction Materials*, 16 (2022) e01052.

[2] Y. Yang, D. Pan, G. Wu, & D. Cao, "A new design method of the equivalent stress–strain relationship for hybrid (FRP bar and steel bar) reinforced concrete beams," in *Composite structures* 270 (2021) 114099.

[3] W. Tingyan, Z. Yun, & Z. Junwei, "Calculation on Bending Stiffness of RC Short Beam Strengthened by CFRP," in *Advances in Civil Engineering* (2020) 8836284.

[4] S-H Lee, A. Abolmaali, K. Jae Shin, & H-Du Lee, "ABAQUS modelling for post-tensioned reinforced concrete beams," in *Building Engineering* 30 (2020) 101273.

[5] J. A. O. Barros, M. Taheri, & H. Salehian, "A model to simulate the moment–rotation and crack width of FRC members reinforced with longitudinal bars," in *Engineering Structures* 100 (2015) 43–56.

[6] A. K. El-Sayed, E. F. El-Salakawy, & B. Benmokrane, "Shear Capacity of High-Strength Concrete Beams Reinforced with FRP Bars," in *ACI Structural Journal*/May-June V. 103, No. 3 (2006) 383-389.

[7] Z. Huang, W. Chen, T. Tran, T. Pham, H. Hao, Z. Chen, & M. Elchalakan, "Experimental and numerical study on concrete beams reinforced with Basalt FRP bars under static and impact loads," in *Composite structures* 263 (2021) 113648.

[8] O. A. Mohamed & W. Al Hawat, "Keshawarz, M. Durability and Mechanical Properties of Concrete Reinforced with Basalt Fiber-Reinforced Polymer (BFRP) Bars: Towards Sustainable Infrastructure," in *Polymers* 13 (2021), 1402.

[9] O. A. Mohamed, M. A. Kewalramani & A. M. Imran, "Shear and flexure of FRP-reinforced concrete beams and slabs – A review," in *Materials Today* (2023) ISSN 2214-7853.

[10] A. Abushanab, W. Alnahhal & M. Farraj, "Experimental and finite element studies on the structural behavior of BFRC continuous beams reinforced with BFRP bars," in *Composite structures* 281 (2022) 114982.
[11] T. H. Almusallam, "Analytical Prediction of Flexural Behavior of Concrete Beams Reinforced by FRP Bars," in *Composite Materials* (1997) 31: 640.
[12] A. Arabshahi, M. Tavakol, J. Sabzi & N. Gharaei-Moghaddam, "Prediction of the effective moment of inertia for concrete beams reinforced with FRP bars using an evolutionary algorithm," in *Structures* 35 (2022) 684-705.
[13] S-H. Chao, A. E. Naaman & G. Parra-Montesinos, "Bond Behavior of Reinforcing Bars in Tensile Strain Hardening Fiber-Reinforced Cement Composites," in *ACI Structures Journal* (2009) 897-906.
[14] O. Mohamed & H. Zuaiter, "Fresh Properties, Strength, and Durability of Fiber-Reinforced Geopolymer and Conventional Concrete: A Review," in *Polymers* 16 (2024), 141.
[15] A. Abushanab, W. Alnahhal, M. Farraj, "Structural performance and moment redistribution of basalt FRC continuous beams reinforced with basalt FRP bars," in *Engineering Structures* 240 (2021) 112390.
[16] D. M. Rakić, A. Bodic, N. Milivojevic, & V. Dunic, "Concrete Damage Plasticity Material Model Parameters Identification," in *the Serbian Society for Computational Mechanics* 15 (2021) 111-122.
[17] M. Hafezolghorani, F. Hejazi, R. Vaghei, & M. Jaafar, "Simplified Damage Plasticity Model for Concrete," in *Structural Engineering International* (2017) 68-78.
[18] A. Demir, H. Ozturk, K. Edip, M. Stojmanovska, & A. Bogdanovic, "Effect of Viscosity Parameter on the Numerical Simulation of Reinforced Concrete Deep Beam Behavior," in *Journal of Science and Technology* Vol. 8 (2018) 50-56
[19] S. Michał &W. Andrzej, "Calibration of the CDP model parameters in Abaqus," in Structural Engineering and Mechanics (2015).
[20] T. Ayub, N. Shafiq & S. Khan, "Compressive Stress-Strain Behavior of HSFRC Reinforced with Basalt Fibers," in *Journal of Materials in Civil Engineering* (2015) 06015014.
[21] T. Ayub, S. U. Khan & N. Shafiq, "Flexural Modelling and Finite Element Analysis of FRC Beams Reinforced with PVA and Basalt Fibres and Their Validation," in *Advances in Civil Engineering* (2018) 8060852.
[22] M. Kh. Hind, M. Ozakca & T. Ekmekyapar, "A Review on Nonlinear Finite Element Analysis of Reinforced Concrete Beams Retrofitted with Fiber Reinforced Polymers," in *Journal of Advanced Research in Applied Mechanics* Vol. 22, (2016) 13-48.
[23] H. Bian, Y. Guo, Y. Liu & W. Shi, "Investigating stress–strain relationship and damage constitutive model of basalt fibre reinforced concrete under uniaxial compression," in *Journal of Building Engineering* 73 (2023) 106789.
[24] W. Mansour, "Numerical analysis of the shear behavior of FRP-strengthened continuous RC beams having web openings," in *Engineering Structures* 227 (2021) 111451.
[25] Y. W. Zhou, Y. F. Wu, J. G. Teng, & A. Y. T. Leung, "Ductility analysis of compression-yielding FRP-reinforced composite beams" in Cement & Concrete Composites 31 (2009) 682–691.
[26] M. K. Dhahir & W. Nadir, "A compression field-based model to assess the shear strength of concrete beams reinforced with longitudinal FRP bars," in *Construction and Building Materials* 191 (2018) 736–751.
[27] E. Shadafza, and R. Saleh Jalali, "The Elastic Modulus of Steel Fiber Reinforced Concrete (SFRC) with Random Distribution of Aggregate and Fiber," in *Civil Engineering Infrastructures Journal*, 49(1): 21 – 32, June 2016.
[28] H. Chen, W-J. Yi, Z. John Ma, H-J. Hwang, "Modelling of shear mechanisms and strength of concrete deep beams reinforced with FRP bars," *Composite Structures* (2019).
[29] R. Nayal & H. A. Rasheed, "Tension Stiffening Model for Concrete Beams Reinforced with Steel and FRP Bars," in *Materials in Civil Engineering* (2016) 831-841.
[30] H. Madkour, M. Maher, & O. Ali, "Finite element analysis for interior slab-column connections reinforced with GFRP bars using damage plasticity model," in *Journal of Building Engineering* 48 (2022) 104013.
[31] Abaqus Guide 6.13
[32] Yucheng Liu "Choose the Best Element Size to Yield Accurate FEA Results While Reduce FE Model's Complexity," in *British Journal of Engineering and Technology* (2013) 13-28.

[33] A. Torabian, B. Isufi, D. Mostofinejad, & A. Ramos, “Flexural strengthening of flat slabs with FRP composites using EBR and EBROG methods,” in *Engineering Structures* 211 (2019) 110483.
[34] E. Najaf, M. Orouji, & K. Ghouchani, “Finite element analysis of the effect of type, number, and installation angle of FRP sheets on improving the flexural strength of concrete beams,” in *Construction Materials* 17 (2022) e01670.
[35] M. Kewalramani, O. Mohamed, and A. Badran, “Parametric finite element analysis to investigate flexural behavior of BFRP-FRC beams,” E3S Web Conf., 347 (2022) 2006.
[36] O. Mohamed and R. Khattab, “Review of Punching Shear Behaviour of Flat Slabs Reinforced with FRP Bars,” 2017 IOP Conf. Ser.: Mater. Sci. Eng. 245 032064